Volume 16, Issue 1, 162504 (1-12)

International Journal of Nano Dimension (IJND)

https://dx.doi.org/10.57647/j.ijnd.2025.1601.04

A comprehensive, computational study framework of the influence of aluminum oxide nanoparticles on double-diffusive convection in a lid-driven enclosure

Najmeh Hajialigol[1]*, Abolfazl Fattahi[2], Hamidreza Shahbazian[2]

[1]*Department of Mechanical Engineering, Hamedan University of Technology, Hamedan, Iran.*
[2]*Faculty of Mechanical Engineering, University of Kashan, Kashan, Iran.*

*__Corresponding author:__ n.hajialigol@hut.ac.ir

Original Research

Received:
21 August 2024
Revised:
28 September 2024
Accepted:
29 September 2024
Published online:
10 January 2025

Abstract:

The current investigation emphasizes the Aluminum oxide in water nanoparticles' effect on double-diffusive mixed convection flow in lid-driven enclosure numerically. The main purpose of the investigation is the assessment of the changes in heat and transfer, due to variations of the dimensionless parameters of the Richardson number that covers the range of 0.01 and 100, the Lewis number that changes from 0.1 to 10, also 0 to 5 are related to the changes of the buoyancy ratio and the nanoparticles volume fraction is fallen in the range of 0 to 0.06 and the location displacement of the source from the highest to lowest in the left wall. The control volume method, SIMPLER algorithm, and a hybrid discretization method are applied to the governing equations. The fluctuations of the mean Nusselt number as well as the mean Sherwood numbers via the variation of the mentioned dimensionless numbers are illustrated. The results indicate that heat transfer is enhanced with increasing nanoparticle concentration, while mass transfer is subsided. Moreover, the rate of both heat and mass transfer is amplified by up to 25% as the buoyancy ratio increases from 0 to 5. However, the Richarson number increment makes a decrement in both.

Keywords: Al_2O_3-water nanofluid; Double-diffusion; Heat transfer augmentation; Mixed convection; Nusselt number; Sherwood number

1. Introduction

The development of advanced heat exchangers, air conditioning systems, and industrial processes has been heavily influenced by research on mixed convective heat transfer in recent years [1, 2]. Double-diffusive convection is the simultaneous heat and mass transfer and so temperature as well as gradients of concentration are two influencing factors on buoyancy-driven flow [3, 4]. Notably, the two buoyancy forces can be effective in aiding or opposing the flow directions. Double diffusion happens in numerous industrial and environmental processes. This can happen in thermal management systems, such as electronics cooling, heat exchangers, and thermal energy storage devices. Furthermore, chemical processing and separation that involve both thermal and solutal gradients, for instance, drying, distillation, and adsorption are the other applications. Air circulation in buildings, heat and mass transfer in lakes and oceans, and the dynamics of porous media like soil and aquifers that happen in environmental and geophysical processes as well as transport of nutrients and metabolites in living organisms, and drug delivery occurred in biological systems are the other instance for double-diffusion applications. Additionally, materials processing where the use of nanoparticles can potentially improve the efficiency of the processing techniques, such as casting, sintering, and additive manufacturing are the further applications.

Deng et al. [5] examined the phenomenon of double-diffusive mixed convection in a 2D and laminar regime within a ventilated enclosure. Their outcomes were presented in the streamlines, heatlines and masslines forms. They tried to minimize heat and mass transfer by proposing a correlation between Reynolds and Grashof numbers. Al-Amiri et al. [6] analyzed the combined influence of diffusion of thermal and mass on mixed steady-state convection in a square cavity driven by a moving lid. In their research, the Galerkin weighted residual method was used for numerical solving of the transport equations. Their results illustrated the specific range in which the highest rate of heat and mass

Nomenclature			
c	Concentration	U_p	Movable plate velocity
C	Dimensionless concentration	x,y	Cartesian coordinates
D	Mass diffusivity	X,Y	Dimensionless Cartesian coordinates
H	Height of Enclosure	Y_D	Source location
L	Thickness of enclosure	**Greek symbols**	
Le	Lewis number (Sc/Pr)	α	Thermal diffusivity
N	Buoyancy ratio	θ	Dimensionless temperature
Nu	Nusselt number	φ	Volume fraction
p	Pressure	β	Volumetric coefficient
P	Dimensionless pressure	**Subscript**	
Pr	Prandtl number	avg	average
Ra	Rayleigh number	c	Cold wall
Ri	Richardson number	h	Hot wall
Sh	Sherwood number	T	Thermal
T	Temperature	M	Mass
u,v	Components of velocity	nf	Nanofluid
U,V	Dimensionless velocity components	p	Particle

transfer is achieved when the Richardson number equals a certain threshold. Beya and Lili [7] investigated numerically a double-diffusive mixed convection in a room under ventilation. The convection was determined oscillatory. The oscillation conditions for the flow inside the room were indicated using a non-linear relation between Reynolds and Grashof numbers. A computational method study about a cavity in a rectangular shape equipped with lid-driven in the mixed convection condition was performed by Teamah and El-Maghlany [8]. The authors studied the dependence of the Richardson number, Lewis number, and buoyancy ratio on the characteristics of iso-contours, streamlines, and temperature distributions. The spread of Richardson numbers and buoyancy ratios was extensive, covering a range of 0.01 to 104 and -10 to 10, respectively. Their findings clearly expressed that when buoyancy ratio values were negative, the Nusselt number in opposing flow was more than assisting flow at the high Richardson number.

Tizakast et al. [9] examined the dynamics of double-diffusive mixed convection in a horizontal enclosure in a rectangular shape occupied with non-Newtonian fluids, using a Rayleigh-Bénard setup. Upscaling the Peclet number intensified fluid flow, the rate of heat transfer and mass transfer accelerated initially but then stabilized at a constant level. Increasing the Lewis number, buoyancy ratio, and thermal Rayleigh number empowered the natural convection. A critical Peclet number that changed the transfer regime was determined, influenced by multiple variables, for instance, Lewis number, buoyancy ratio, and thermal Rayleigh number. Gnanasekaran and Satheesh [10] conducted a mathematical investigation on the impact of magnetic fields on double-diffusive convection in a cavity with thermal and solutal sources. The independent parameters were chosen including Lewis number, Hartmann number, Reynolds number, and some geometrical parameters. An increment in the Reynolds number improved the rates of heat transfer and mass transfer, despite that the Hartmann number diminished it. Increasing the Lewis number had a double-faced outcome on the heat transfer as well as mass transfer. Changing the source location could lead to a rise in heat and mass transfer rates. They developed empirical correlations for the mean heat transfer coefficient and mass transfer coefficient.

As limited specific heat capacity and thermal conductivity of fluids like water, air, and ethylene glycol are fundamentally the main restrictions against convective heat transfer coefficient improvement, therefore dispersion of diverse sorts of nano-sized solid particles in a base fluid called a nanofluid, can be an applicable method to dominate this limitation [11, 12]. Ben-Nakhi and Chamkha [13] assessed laminar natural convection in a cavity with an inclined fin attached with varying lengths. A mixed convection flow in laminar conditions filled with a nanofluid including copper nanoparticles and water was investigated in a cavity in a square shape equipped with a lid-driven by Talebi et al. [14]. Selected solid volume fraction, Reynolds number, and Rayleigh number in the study were 0 to 0.05, 1 to 100, and 10^4 to 10^6 respectively. The thermal conductivity was estimated by Patel models and the Brinkman model was employed to calculate the effective viscosity of the nanofluid, similarly. The outcomes show that as the Reynolds number increased, the solid concentration effect decreased. In a separate study, Nemati et al. [15] researched the effect of Cu, CuO, or Al_2O_3-water as nanofluids on heat transfer improvement in mixed convection flow at a boundary-driven cavity by applying the Lattice Boltzmann technique. Their published outcomes revealed a consistent trend of increasing effects of solid volume fraction for Al_2O_3, CuO, and Cu nanoparticles, with each subsequent material exhibiting a stronger influence.

Chamkha and Abu-Nada [16] mathematically simulated a laminar convection flow at individual and paired-lid cavities. They found that a significant increment in heat transfer can be obtained due to the nanoparticles attendance and moderate to large Richardson numbers, accompanied by increasing nanoparticle volume fractions, intensify this phenomenon. In another study, the role of various properties of nanofluid was investigated by Abu-Nada et al. [17]. In the research, the enclosure has warmed up differentially. The authors investigated the impact of the physical and thermal properties of nanofluid and found that they play a determinative role in the estimation of the improvement of heat transfer. Mahapatra et al. [18] delved into the Darcian and non-Darcian law for natural convection fluid flow in a porous cavity under the influence of thermal radiation. It was illustrated that the radiation heat transfer made no

considerable effect on the thermal profile and fluid flow, however, it stood for the variations in the Nusselt number. Mahapatra et al. [19] considered the effect of thermal radiation on mixed combustion in a partially heated cavity. The magnetic field magnitude was shown to be an outstanding parameter for the heat and mass transfer patterns.

Mondal and Sibanda [20] investigated simultaneous heat and mass transfer in an inclined cavity in unsteady conditions. The results showed the magnetic angle and inclination cavity angle were the imperative parameters for thermal and solutal fields. In another study [21] , they investigated the unsteady double-diffusion problem in a porous cavity by varying buoyancy ratio. A theoretical investigation on the double-diffusive convective flow at a stagnation-point area contained with nanofluid, accounting for the diffusiophoresis impact of the binary base fluid, was carried out by Dinarvand et al. [22] using an analytical-numerical method. The effects of Numerous aspects, such as the mixed convection characteristic, nanofluid buoyancy ratio, regular double-diffusive buoyancy parameter, thermophoresis specification, and Brownian coefficient, concerning temperature and velocity scaling as well as a concentration of nanoparticles were investigated. The results show that an increment in the mixed convection characteristic enhanced the velocity and reduced the temperature and concentration profiles. As the nanofluid buoyancy ratio increased, the trend reversed, with a contrasting effect observed when the regular double-diffusive buoyancy parameter was raised.

Abbasian Arani et al. [23] investigated the double-diffusive mixed convection in a boundary-driven enclosure in a square shape filled with an alumina-water nanofluid. The simulations spanned a range of Richardson numbers between 0.01 and 100, buoyancy ratios ranging from -5 to 5, and nanomaterial volume percentages in the range of 0 to 4% as well as considering temperature-dependent properties. The findings indicated that increasing the nanoparticle concentration left an opposite effect on the mean Nusselt number over a wide range of Reynolds numbers. Further, the positive buoyancy ratios consistently yielded higher average Nusselt or Sherwood numbers compared to those of negative values. The authors concluded higher convective heat transfer of nanofluids in contrast to the main fluid by considering the heatlines' compactness. Ahamed et al. [24] investigated nanofluid flow in the presence of an electrical and magnetic field in unsteady conditions passing over an inclined cylinder, while Ohmic dissipation was calculated. The mass gradient and temperature field are among the results presented. Hussain et al. [25] studied double-diffusive mixed convection in a porous enclosure in a square shape contained with an alumina-water nanofluid of water and alumina, numerically. A hybrid approach was used, involving solving the governing equations using a monolithic Galerkin finite element method in conjunction with a geometric multigrid technique. Besides those parameters commonly used for such problems, porosity, chemical reaction parameters, and geometrical parameters were involved.

Alsabery et al. [26] investigated a double lid-driven filled with alumina-water nanofluid considering Buongiorno's two-phase model. The range for the Reynolds and Richardson numbers are respectively 1 to 500 and 0.01 to 100. The results indicated that suspending nanoparticles in low Reynolds number and high Richardson number left a decreasing effect on the Nusselt number. A study by Nath and Krishnan [27] explored the numerical examination of thermo-solutal buoyancy-driven fluid convection in a backward-facing step channel contained with copper-water nanofluid. Galerkin's finite element method was applied. The mean Sherwood numbers and Nusselt numbers respectively enhanced and mitigated by 34% and 77%, if nanoparticle volume concentration increased from 0.0 to 20%.

Dogonchi et al. [28] numerically investigated the MHD problem in an enclosure filled with a nanofluid and featured with wavy walls. The contraction ratio of the wavy wall abated the convective heat transfer. Chamkha and Al-Naser [29] conducted an unsteady, laminar double-diffusive flow in a cavity of porous media. Thermal and solutal buoyancy acted in an opposite direction and the effect of Darcy number and inclination of the cavity were studied. Hashemi-Tilehnoee et al. [30] analyzed the first and second laws of thermodynamics for a cavity with a wavy heater having alumina-water nanofluid underinfluencing a magnetic field. The entropy generation number and Nusselt number showed a monotonic trend with the Rayleigh number and the Darcy number. Alomari et al. [31] presented a numerical investigation into the double-diffusive mixed convection of a MWCNT/water mixture in an enclosure characterized by a curvilinear geometry and hot elliptical sources. It was shown that increasing Reynolds, Richardson, and Lewis numbers resulted in an increment in the Nusselt and Sherwood numbers. At low Richardson and Reynolds numbers of respectively 0.1 and 50, the mean Nusselt number and mean Sherwood number were found to be 7.4 and 10.7.

Jalili et al. [32] investigated the mixed convection flow in a channel with the vertical form filled with a nanofluid using analytical methods. They tried finding some features of more efficient heat transfer in devices included with nanofluid. Brownian motion and thermophoresis were monitored. The proposed analytical techniques showed excellent agreement with a numerical method, confirming their accuracy and reliability. Parveen et al. [33] performed a quantitative investigation into the double-diffusive mixed convection in a container filled with Fe_3O_4-water ferrofluid by utilizing magnetic induction. The container involved a thermal source/sink. The researchers attempted to augment the thermal-solutal behavior. As the Hartmann number increased, heat and mass transfer rates declined, whereas they rose with growing buoyancy ratio, Richardson number, and inclination angle. By a twice increment of in the thermal generation from 5 to 10, the Nusselt number raised 3.5 folds. Devi et al. [34] studied the double-diffusive mixed convection in the presence of magnetic force and a nanofluid of Fe_3O_4 and water in a square cavity. In the given configuration, elevated temperatures and concentrations were recorded inside the square blockages, with contrasting conditions prevailing on the left and right walls. The incorporation of a nanoparticle resulted in a more significant impact on fluid flow dynamics compared to thermal and solutal effects. Unlike commonly expected, enhancing the

nanoparticle volume fraction resulted in a reduction of the average Nusselt and Sherwood numbers at larger Richardson numbers.

As stated above, while mixed convection has been widely studied, the inclusion of double-diffusion of heat and mass transfer makes the phenomenon more realistic and closer to real-world scenarios. This provides more accurate predictions for systems involving coupled transport phenomena. Studying such topics provides more precise predictions for systems involving dual transport phenomena. Involving nanoparticles in the thermal system is beneficial; however, the effect of nanoparticles on the solutal field needs to be more investigated. In the current study, mixed convection in a boundary-driven container in a square shape involved with Al_2O_3-water nanofluid is explored in the CFD-based method. Unlike previous studies that used constant nanoparticle properties, the current work considers the temperature-dependent thermal and physical features of the Al_2O_3 nanoparticles. This leads to a more precise numerical simulation and a better understanding of the effects of nanoparticles on the flow, heat, and mass transfer processes. The main objectives of the present work, therefore, are:

• To numerically investigate mixed convection in a boundary-driven square container involving the nanofluid, considering the temperature-dependent thermal and physical properties of the nanoparticles.

• To study the effects of key parameters, such as Richardson number, Lewis number, buoyancy ratio, and nanoparticle volume fraction on the resulting flow field, heat transfer, and mass transfer.

• To provide a more comprehensive understanding of the underlying physics, especially in real phenomena, and the influence of these parameters on the mixed convection phenomenon with double-diffusion of heat and mass.

• To demonstrate the practical relevance of these findings by discussing their implications for the design of engineering systems involving coupled heat and mass transfer.

2. Materials and Methods

2.1 Physical model and the problem formulation

Fig. 1 depicts schematically the computational domain of the present research. The boundary condition of the wall on the left side includes a source with high temperature and concentration (T_h,C_h), while the wall on the right side experiences a low temperature and concentration (T_c,C_c). According to Fig. 1, the boundary condition of the left wall is applied only to half of the wall (L/2). Correspondingly, the insulating and impermeable boundary condition is considered for the horizontal top and the bottom walls, as well as, the inactive section of the left wall of the computational domain. The boundary condition for the top wall of the enclosure is constant velocity to the right direction (U_p).

The center of the source respect to the left wall is characterized by the dimension of h. The dimensionless variable, Y_D for the Source location, is defined as $Y_D = h/L$.

In the domain of numerical solution, the Boussinesq approximation is established by supposing a linear relationship between density, temperature, and concentration, as follows.

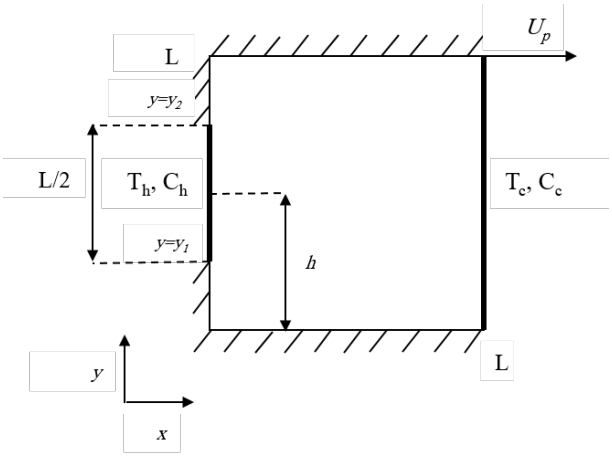

Figure 1. Physical model and the boundary conditions of the present study.

$$\rho = \rho_0(1-\beta_T(T-T_c)-\beta_M(c-c_\tau)) \tag{1}$$

The enclosure is filled with nanofluid including the water as the base flow and Al_2O_3 as nanoparticles. The assumptions of the current work are as follows.

• The fluid is Newtonian, incompressible, and viscous.

• The viscous dissipation is negligible.

• The influences of the Dufour and Soret effects, which describe the mass transport caused by temperature gradient and heat flux caused by concentration gradients, respectively, are ignored.

• The fluid phase and nanoparticles have identical velocities and are in thermal equilibrium.

• A uniform shape and size are considered for the nanoparticles.

The properties of the nanofluid, including thermal conductivity and viscosity, are influenced by the nanoparticle volume fraction and temperature. Assuming these conditions, the system's governing equations are given as follows:

Continuity equation

$$\frac{\partial u}{\partial x}+\frac{\partial v}{\partial y}=0 \tag{2}$$

x-momentum equation:

$$\rho_{nf}(u\frac{\partial u}{\partial x}+v\frac{\partial u}{\partial y}) = -\frac{\partial p}{\partial x}+\frac{\partial}{\partial x}(\mu_{nf}\frac{\partial u}{\partial x})+\frac{\partial}{\partial y}(\mu_{nf}\frac{\partial u}{\partial y}) \tag{3}$$

y-momentum equation::

$$\rho_{nf}(u\frac{\partial v}{\partial x}+v\frac{\partial v}{\partial y}) = -\frac{\partial p}{\partial y}+\frac{\partial}{\partial x}(\mu_{nf}\frac{\partial v}{\partial x})+\frac{\partial}{\partial y}(\mu_{nf}\frac{\partial v}{\partial y})+$$
$$[\varphi\rho_p\beta_{T_\rho}+(1-\varphi)\rho_f\beta_{T_f}]g(T-T_c)+ \tag{4}$$
$$[\varphi\rho_p\beta_{M_\rho}+(1-\varphi)\rho_f\beta_{M_f}]g(c-c_c)$$

Energy equation:

$$(\rho c_p)_{nf}(u\frac{\partial T}{\partial x}+v\frac{\partial T}{\partial y}) = \frac{\partial}{\partial x}(k_{nf}\frac{\partial T}{\partial x})+\frac{\partial}{\partial y}(k_{nf}\frac{\partial T}{\partial y}) \tag{5}$$

Concentration equation:

$$u\frac{\partial c}{\partial x}+v\frac{\partial c}{\partial y}=\frac{\partial}{\partial x}(D\frac{\partial c}{\partial x})+\frac{\partial}{\partial y}(D\frac{\partial c}{\partial y}) \quad (6)$$

The nanofluid effective density at the reference temperature is defined by:

$$\rho_{nf}=(1-\varphi)\rho_f+\varphi\rho_{p.0} \quad (7)$$

and the nanofluid-specific heat capacity is given as

$$(\rho\beta)_{nf}=(1-\varphi)(\rho\beta)_f+\varphi(\rho\beta)_p \quad (8)$$

$$(\rho c)_{nf}=(1-\varphi)(\rho c_p)_f+\varphi(\rho c_p)_p \quad (9)$$

The nanofluid effective thermal conductivity by using model of the Chon et al. [35, 36] is derived by

$$\frac{k_{nf}}{k_f}=1+64.7\varphi^{0.4076}(\frac{d_f}{d_p})^{0.3690}(\frac{k_p}{k_f})^{0.7476}Pr_T^{0.9955}Re^{1.2321} \quad (10)$$

where Pr_T and Re are:

$$Pr_T=\frac{\mu_f}{\rho_f\alpha_f} \quad (11)$$

$$Re=\frac{\rho_f k_b T}{3\pi\mu_f l_f} \quad (12)$$

in which k_b=1.3807×10^{-23} J/K, is the Boltzmann constant and l_f=0.17 nm is the mean path of fluid particles [16, 17]. The nanoparticle viscosity is calculated by Nguyen et al. [36] and also used by Ref. [37]

$$\mu_{nf}=\exp(30.003-0.04203T-0.5445\varphi+0.0002553T^2+$$
$$0.0524\varphi^2-1.622\varphi^{-1})\times10^{-3} \quad (13)$$

The temperature-dependent viscosity of base fluid (water) is calculated using the following equation [17, 22]:

$$\mu_f=(1.2723\ln^5 T-8.736\ln^4 T+33.708\ln^3 T-246.6\ln^2 T+$$
$$518.78T\ln T+1153.9)\times10^{-6} \quad (14)$$

Using the Grashof number and Reynolds number, the Richardson number reads as

$$Ri=\frac{Gr}{Re^2}$$
$$Gr=\frac{gL^3\beta\Delta T}{U^2} \quad (15)$$

The following dimensionless variables are defined to express the governing equations in a dimensionless form.

$$X=\frac{x}{L}$$
$$Y=\frac{y}{L}$$
$$U=\frac{u}{L}$$
$$V=\frac{v}{U_p}$$
$$P=\frac{p}{\rho_{nf}U_\rho^2} \quad (16)$$
$$\theta=\frac{T-T_c}{T_h-T_c}$$
$$C=\frac{c-c_c}{c_h-c_c}$$

The governing equation with the dimensionless form can be formulated as the following equations.
Continuity equation:

$$\frac{\partial U}{\partial X}+\frac{\partial V}{\partial Y}=0 \quad (17)$$

x-momentum equation:

$$U\frac{\partial U}{\partial X}+V\frac{\partial V}{\partial Y}=-\frac{\partial P}{\partial X}+\frac{\partial}{\partial X}(\frac{1}{Re^*}\frac{\partial U}{\partial X})+\frac{\partial}{\partial Y}(\frac{1}{Re^*}\frac{\partial V}{\partial Y}) \quad (18)$$

y-momentum equation:

$$U\frac{\partial U}{\partial X}+V\frac{\partial V}{\partial Y}=$$
$$-\frac{\partial P}{\partial X}+\frac{\partial}{\partial X}(\frac{1}{Re^*}\frac{\partial U}{\partial X})+\frac{\partial}{\partial Y}(\frac{1}{Re^*}\frac{\partial V}{\partial Y}+Ri^*(\theta+NC)) \quad (19)$$

Energy equation:

$$U\frac{\partial \theta}{\partial X}+V\frac{\partial \theta}{\partial Y}=$$
$$\frac{1}{\alpha_f\times(\rho c_p)_{nf}}[\frac{\partial}{\partial X}(\frac{k_{nf}}{Re^*Pr^*}\frac{\partial \theta}{\partial X})+\frac{\partial}{\partial Y}(\frac{k_{nf}}{Re^*Pr^*}\frac{\partial \theta}{\partial Y})] \quad (20)$$

Concentration equation:

$$U\frac{\partial C}{\partial X}+V\frac{\partial C}{\partial Y}=$$
$$\frac{\partial}{\partial X}(\frac{1}{Le^*Re^*Pr^*}\frac{\partial C}{\partial X})+\frac{\partial}{\partial Y}(\frac{1}{Le^*Re^*Pr^*}\frac{\partial C}{\partial X}) \quad (21)$$

where

$$Pr^*=\frac{\mu_{nf}}{\mu_f}\frac{C_{P_{nf}}}{C_{P_f}}\frac{k_f}{k_{nf}}Pr$$
$$Le^*=\frac{\rho_f}{\rho_{nf}}\frac{C_{p_f}}{C_{p_{nf}}}\frac{k_{nf}}{k_f}Le$$
$$Re^*=\frac{\rho_{nf}}{\rho_f}\frac{\mu_f}{\mu_{nf}}Re$$
$$Ri^*=\frac{(\rho\beta)_{nf}}{\rho_{nf}\beta_f}Ri$$

Boundary conditions in non-dimensionalized form are

$$X=0,0\le Y\le1:U=V=0,$$
$$\theta=C=1,\quad \text{on the source section}$$
$$\frac{\partial\theta}{\partial n}=\frac{\partial C}{\partial n}=0,\quad \text{on the inactive portion}$$
$$X=1,0\le Y\le1:$$
$$U=V=0,\theta=C=0 \quad (22)$$
$$Y=0,0\le X\le1:U=V=0,\frac{\partial\theta}{\partial n}=\frac{\partial C}{\partial n}=0,$$

$$Y = 1, 0 \le X \le 1 :$$
$$U = 1, V = 0, : \frac{\partial \theta}{\partial n} = \frac{\partial C}{\partial n} = 0$$

where $\partial / \partial n$ expresses the normal direction derivative. Also, The average Nusselt and Sherwood numbers have been estimated from the below equations:

$$Nu_{avg} = -2\frac{k_{nf}}{k_f}\int_{Y_1}^{Y_2} \frac{\partial \theta}{\partial X}|_{X=0} dY \quad (23)$$

$$Sh_{avg} = -2\int_{Y_1}^{Y_2} \frac{\partial C}{\partial X}|_{X=0} dY \quad (24)$$

where $Y_1 = y_1/L$ and $Y_2 = y_2/L$. The coordinates y_1 and y_2 are defined and depicted in Fig. 1.

2.2 Numerical method

Non-linear governing equations are solved using the finite volume technique, with suitable boundary conditions applied. The well-known SIMPLER algorithm is applied in order to the pressure and velocity field coupling in the momentum equations. A structured uniform mesh is utilized for the current investigation. The system of linear algebraic equations has been successfully solved using TDMA (Three Diagonal Matrix Algorithm) with relaxation factors of 0.6 for velocity, 0.4 for energy, and 0.4 for concentration equation.

2.3 Benchmarking of the code

Seven mesh sizes for the numerical model with 51×51, 91×91, 131×131, 171×171, 211×211, 251×251and 291×291 cells have been applied for the independence survey, respectively. For all the grid studies, the average Nusselt and Sherwood numbers have been calculated. Accordingly, the mesh size of 251×251 is suitable for ensuring the accuracy of numerical solutions based on the mesh independence test.

A comparison between the current results and those obtained by Teamah and El-Maghlany [8] and Esfahani and Bordbar [38] has been made and depicted in Figs. 2 and 3. It is clear that the two sets of results are in good agreement and therefore, the current computer code can capture the sought physics.

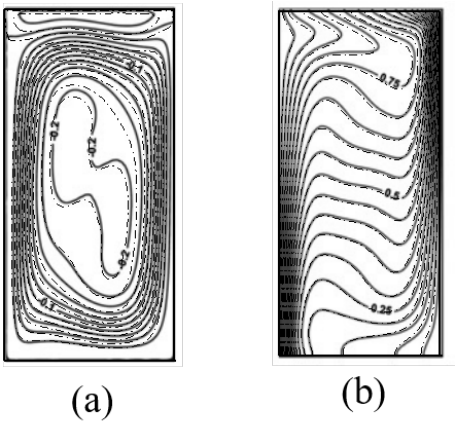

Figure 2. (a) Streamline and (b) isotherm for Le=1, N=10, Ri=1 and U_{up}= -1;Ref. [8] (solid lines), present work(dash lines).

3. Results and discussion

The change of thermal, flow, and solutal field in a boundary-driven enclosure in square shape is numerically investigated based on the variation of buoyancy ratio, Lewis number, Richardson number,and the source location on the double-diffusive mixed convection. The buoyancy ratio differs between 0 to 5, the Lewis number ranges from 0.1 to 10, the Richardson number changes from 0.01 to 100, the nanoparticles volume fraction varies from 0 to 0.06, and the source location shifts from the top of the wall to the bottom, along the left side. It is noted that a base fluid Prandtl number of 5.83 is considered for all the results presented in Figs. 2a, b, and 3.

The influence of N on isotherms, streamlines, and iso-concentrations for Ri=1, Le=1, Y_D=0.5, and different nanoparticle volume fractions have been demonstrated in Fig. 4. The top surface of the enclosure is drifting towards the right and then an induced secondary flow is created with a center near the moving wall. Consequently, natural convection that arises from the temperature gradient between the hot and cold sources, and forced convection intensify each other's effects.

3.1 Effect of the buoyancy ratio

From Fig. 4, it is clear that when φ=0.0 and Le=1, the isotherms and iso-concentrations show the same behavior because of the similarity between the concentration and energy equations. As an interesting point, while N >0, the solutal and thermal buoyancy forces operate in the same direction. At N=0 and 0.2, the circulating cells are formed from the moving plate. So, solutal and thermal boundary layers are considerably created on the left source and above the right wall.

It indicates that with growing N, no significant changes are observed in the contours when solutal boundary forces are more powerful than thermal boundary forces ($|N| < 1$). At N=5, the nanofluid core cell is smaller than the base fluid core cell where thermal buoyancy forces are stronger than solutal boundary forces. In this condition, the boundary layer is more compact than the corresponding layer of other

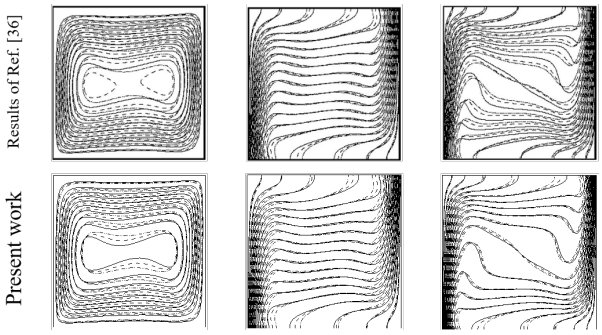

Figure 3. Streamlines, isotherms and iso-concentrations for φ=0.0(solid lines),φ=0.05(dashed lines) andφ=0.1 (dashed-dot-dot lines) at Ra=10^5 and Le=2: the comparison between the present work and the results of Ref. [38].

N cases. This demonstrates that compared to all the cases, the maximum heat transfer and mass transfer happen in the case of *N*=5. Also, a unicellular shape for streamlines can be seen in all *N* values.

The effect of nanoparticle volume fraction on the variation of the average Nusselte number and average Sherwood number in different buoyancy ratios is presented in respectively Figs. 5a, and b. As it is evident, at *N*=0 and 0.2, the values of the average Nusselte number and average Sherwood number are not significantly different from each other. By increasing N, improvement of heat and mass transfer are expected. It is such that by increasing the buoyancy ratio from 0 to 5, the average Nusselt and Sherwood number increases from 20 to 25%, on average, in various nanofluid volume fractions. Further, the increase in nanoparticle volume fraction has been found to lead to a significant improvement in the average Nusselt number due to an important rise in thermal conductive features of the base fluid suspended by nanoparticles.

Despite the increasing mean Nusselt number, the mean Sherwood number shows a contradictory and decreasing behavior against the addition of nanoparticles. It is due to increasing concentration by adding nanoparticles and consequently, decreasing the concentration gradient. While the decrement in average Sherwood number is about 10%, on average, the average Nusselt number increases by about 20%, by increasing the nanoparticles concentration from zero to 0.06. The Nusselt number and Sherwood number exhibit a higher slope when the volume fraction of nanofluid is higher and the buoyancy ratio is increased, highlighted more for the former.

3.2 Effect of Lewis number

The dimensionless Lewis number is determined as a criterion of the ratio of thermal diffusivity to mass diffusivity. Lewis number is employed in situations where the fluid experiences both mass transfer and heat transfer at the same time. In the current study, the variation of the Lewis number is from 0.1 to 10. The Lewis number impact on the isotherms, streamlines, and iso-concentrations is illustrated

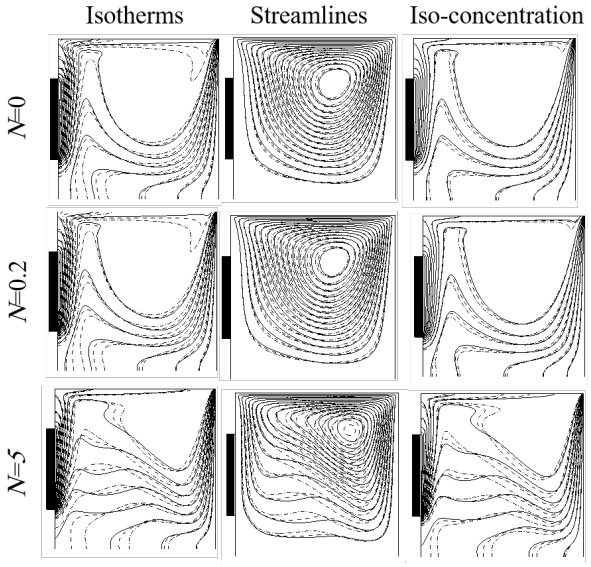

Figure 4. Effect of buoyancy ratio on the isotherms, streamlines and iso-concentrations for various nanoparticle volume fractions:φ=0.0(solid lines),φ=0.03(dash lines),φ=0.006(dash-dot-dot lines) at *Ri*=1, *Le*=1 and Y_D=0.5.

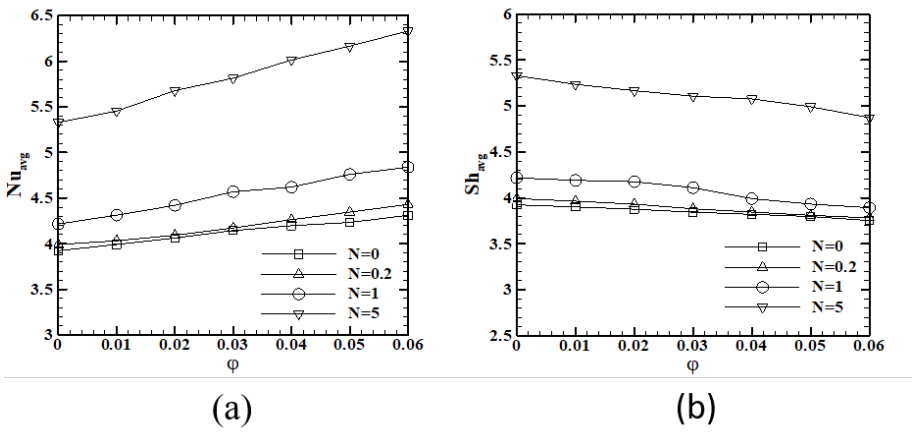

Figure 5. Variation of average (a) Nusselt and (b) Sherwood number versus nanoparticles volume fraction in various buoyancy ratios.

in Fig. 6 at Ri=1, N=1, Y_D=0.5, and various nanoparticle volume fractions.

As can be easily seen, the streamlines will not be significantly affected by the Lewis changes. Streamlines have pre a unicellular structure due to forced and natural convection. At a Lewis number of 0.1, the core of the nanofluid shrinks to a size smaller than the base fluid. However, the thickness of the boundary layer on both the source and top surfaces of the right wall adjusts as the Lewis number varies. The effect of increasing the Lewis number is to render the solutal boundary layer denser and the thermal boundary layer more extensive.

Fig. 7 illustrates the trends of the mean Nusselt number and mean Sherwood number as a function of nanoparticle volume fraction for various Lewis numbers respectively in Figs. 7a, and b. Following Fig. 7(b), nanoparticle volume fraction in low Lewis number does not affect the average Sherwood number, considerably. Furthermore, the variation of the average Sherwood number is lower than the average Nusselt number. Increasing the nanoparticle concentration leads to a declined trend in the mass transfer, which can be clearly observed in Lewis number equal to 10 by 10%. Moreover, because of the densifying solutal boundary layer, an increase in Lewis number has a beneficial impact on mass transfer, which can reach by a factor of 6.6. As soon as the Lewis number rises, mass diffusion diminishes, and based on the continuity equation, forced bulk flow plays the main role in mass transfer. Therefore, the average Sherwood number grows due to the more powerful effect of bulk flow on mass transfer in contrast to molecular diffusion [39]. Conversely, the mean Nusselt number declines with the growth of the Lewis number.

Thermal diffusivity (α=$k/\rho c_p$) improves as the Lewis number rises and it leads to conduction heat transfer to be dominant at a high Lewis number in contrast to the conditions with a low Lewis number. Thus, as the Lewis number rises, the Nusselt number tends to decline because the conduction mechanism becomes weaker compared to the convection mechanism. Increasing the Lewis number from unity to 10 makes the mean Nusselt number to be increased by about

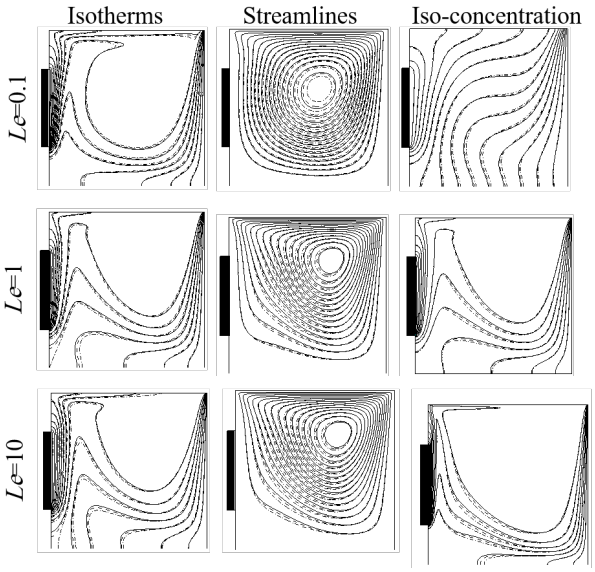

Figure 6. Effect of Lewis number on the isotherms, streamlines, and iso-concentrations for various nanoparticle volume fractions of φ=0.0(solid lines),φ=0.03(dash lines), φ=0.06 (dash-dot-dot lines) at Ri=1, N=1 and Y_D=0.5.

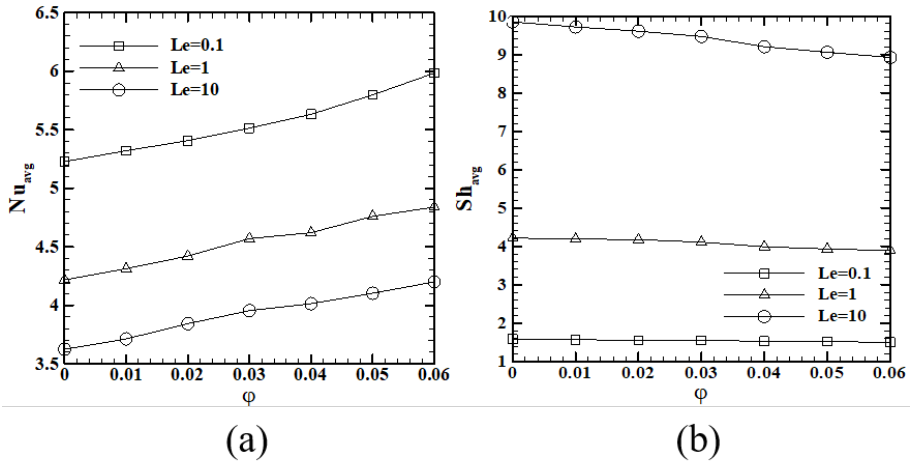

Figure 7. Variation of average (a) Nusselt and (b) Sherwood number versus nanoparticles volume fraction in various Lewis numbers.

25%, on average. It is lower than 20% with increasing the Lewis number from 0.1 to unity. The mean Nusselt number rises by growing nanoparticle volume fraction with a value between 13 to 17%.

3.3 Effect of the Richardson number

The Richardson number indicates the dominance of natural convection over forced convection. In the present investigation, the variation of Richardson number falls in the range of 0.01 and 100. The contours of isotherms, streamlines, and iso-concentrations under the variation of Richardson number are demonstrated in Fig. 8 for different nanoparticle volume fractions in Lewis numbers of 1, N=1, and Y_D=0.5. The Richardson number of 0.01 indicates that forced convection significantly outweighs natural convection. Consequently, the moving plate with a unicellular structure will be formed and affected on the cells. A strong interplay of heat and mass transport occurs across the thin solutal and thermal boundary layers. Natural convection empowers while the Richardson number enhances. As boundary layers become thicker, heat transfer drops like mass transfer. At the Richardson number of 100, in the enclosure core area, it seems to be the dominant mechanism for heat transfer and additionally, the flow core cell expands except for φ=0.06. Figs. 9a, and b present the changes in the parameter of the mean Nusselt number and mean Sherwood number respectively, against nanoparticle volume fractions in diverse Richardson numbers. As it is inferred from the boundary layers thickness, heat, and mass transfer decrease when the Richardson number rises. The trend of the average Nusselt and Sherwood numbers versus nanoparticle volume fraction is semi-linear and for R_i>0.01, the variations can be assumed negligible. By diminishing the Richardson number from 100 to 0.01, the average Nusselt and Sherwood number increases by a factor respectively higher and lower than 3 for φ=0.06. Both show an increment lower than 3 times for the base fluid.

3.4 Effect of the source location

The impact of Y_D on the isotherms, streamlines, and iso-concentrations is displayed in Fig. 10 for several nanoparticle volume fractions at the Lewis number, buoyancy ratio,

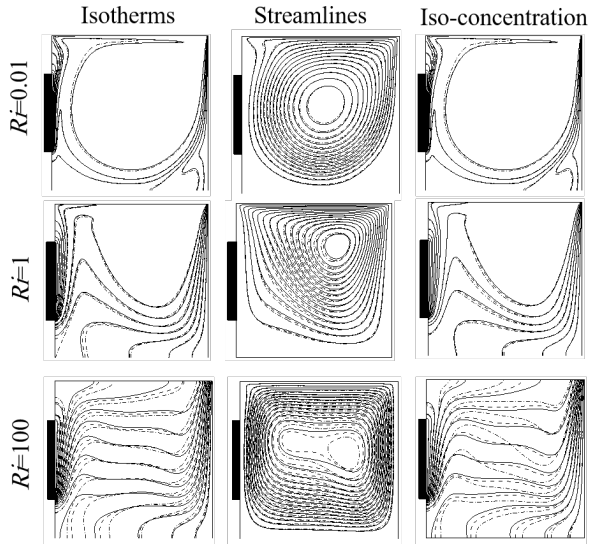

Figure 8. Effect of Richardson number on the isotherms, streamlines, and iso-concentrations for various nanoparticle volume fractions: φ=0.0(solid lines),φ=0.03(dash lines),φ=0.06(dash-dot-dot lines) at Le=1, N=1 and Y_D=0.5.

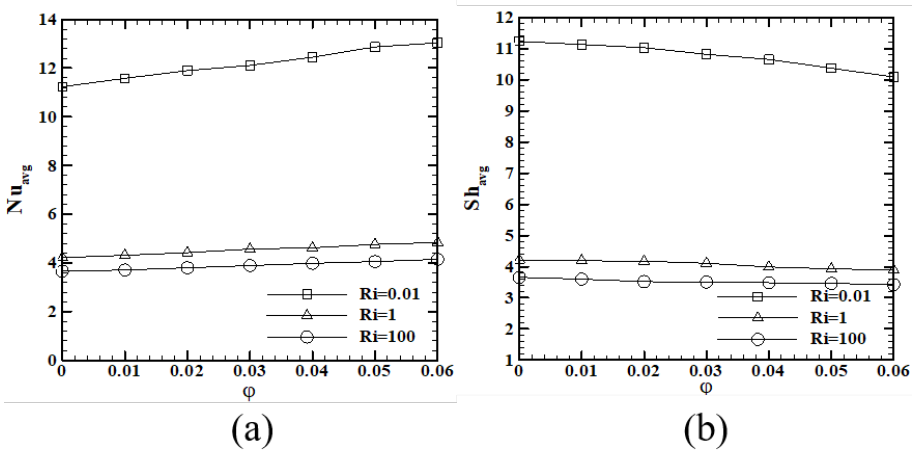

Figure 9. (a, b): Variation of average Nusselt and Sherwood number versus nanoparticle volume fractions in various Richardson numbers.

and Richardson number all equal to unity. By decreasing Y_D by moving the source toward the bottom, the recirculating cells will occupy a wider area of the enclosure. In this situation, as the natural convection grows and rises from the base of the cavity to its upper region, the zones affected by the convection become wider, inferred from both streamlines and isotherms. The mass transfer is not expected.

The variation of the mean Nusselt number and mean Sherwood number against nanoparticle volume fractions in the various source locations is demonstrated in Figs. 11a, b, respectively. It is clear that by decreasing Y_D, the heat and mass transfer are enhanced, earlier concluded from Fig. 10. The intensification in the mean Nusselt number and the mean Sherwood number is respectively 15-25% and 7-13%. By growing the volume fraction, the difference in the mean Nusselt and Sherwood numbers among the cases with various Y_D becomes lower.

4. Conclusion

In the present study, a numerical framework was established so that double-diffusive mixed convection in an enclosure containing a nanofluid included with Al_2O_3 and water with a moving top plate was investigated. Referring to the comprehensive numerical results, the conclusions can be summarized as follows.

- The buoyancy ratio had a positive effect on heat and mass transfer, so heat and mass transfer concurrently increased by increasing the buoyancy ratio from 0 to 5 by a value of 20 to 25%.
- Nanoparticle volume fraction left different effects on the mean Nusselt and Sherwood numbers, as increasing the nanoparticle volume fraction increased the mean Nusselt number and simultaneously decreased the mean Sherwood number. Both could touch the changes of respectively 20% and 10%.
- Lewis number also acted dually on the mean Nusselt and Sherwood numbers. As the Lewis number increased, the mean Sherwood number increased, while the average Nusselt number decreased. The effect of the Lewis number on mass transfer was more considerable than that on the heat transfer. It was such that the former could involve a factor of 6.6 and the latter changed up to 25%.
- The enhanced Richardson number caused a reduction in the amount of heat and mass transferred.
- The positioning of the source at the bottom of the left-hand wall resulted in maximum heat and mass transfer.

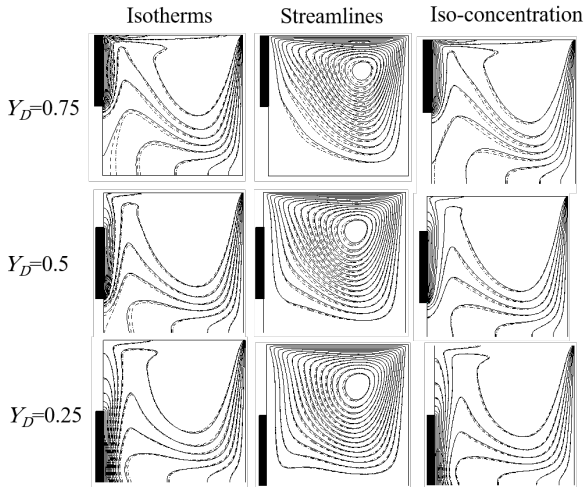

Figure 10. Effect of the source location on the isotherms, streamlines, and iso-concentratioat at Le=1, N=1 and Ri=1.

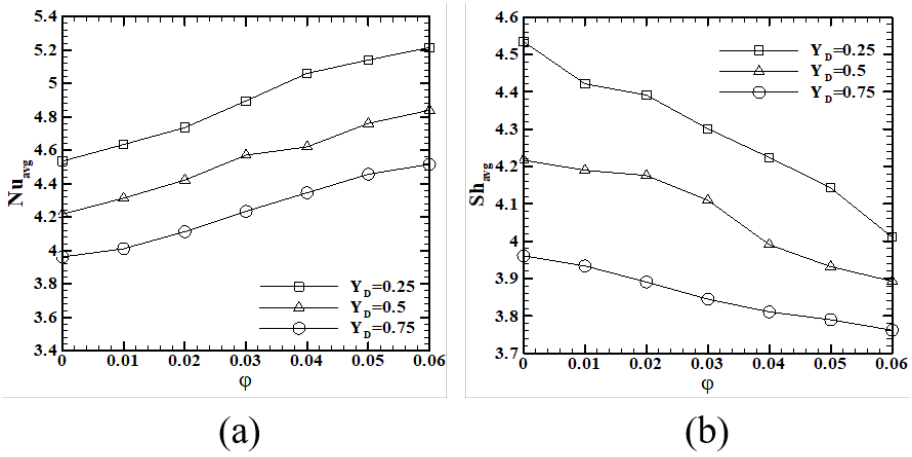

Figure 11. (a, b): Variation of average Nusselt and Sherwood number versus nanoparticle volume fractions in the various source locations.

Authors contributions
Authors have contributed equally in preparing and writing the manuscript.

Availability of data and materials
The data that support the findings of this study are available from the corresponding author, upon reasonable request.

Conflict of interests
The authors declare that they have no known competing financial interests or personal relationships that could have appeared to influence the work reported in this paper.

References

[1] B. Gebhart and L. Pera. The nature of vertical natural convection flows resulting from the combined buoyancy effects of thermal and mass diffusion. *Int. J. Heat Mass Transf*, 14:2025–2050, 1971. DOI: https://doi.org/10.1016/0017-9310(71)90026-3.

[2] A. Bejan. Mass and heat transfer by natural convection in a cavity. *Int. J. Heat Fluid Flow*, 6(3), 1985. DOI: https://doi.org/10.1016/0142-727X(85)90002-5.

[3] C. Beghein, F. Haghighat, and F. Allard. Numerical study of double-diffusive natural convection in a square cavity. *Int. J. Heat Mass Transf*, 35:833–846, 1992. DOI: https://doi.org/10.1016/0017-9310(92)90251-M.

[4] A. J. Chamkha and H. Al-Naser. Hydromagnetic double-diffusive convection in a rectangular enclosure with opposing temperature and concentration gradients. *Int. J. Heat Mass Transf*, 45:2465–2483, 2002. DOI: https://doi.org/10.1016/S1290-0729(02)01386-8.

[5] Q. H. Deng, J. Zhou, C. Mei, and Y. M. Shen. Fluid, heat and contaminant transport structures of laminar double-diffusive mixed convection in a two-dimensional ventilated enclosure. *Int. J. Heat Mass Transf*, 47(24):5257–5269, 2004. DOI: https://doi.org/10.1016/j.ijheatmasstransfer.2004.06.025.

[6] A. M. Al-Amiri, K. M. Khanafer, and I. Pop. Numerical simulation of combined thermal and mass transport in a square lid-driven cavity. *Int. J. Therm. Sci*, 46(7):662–671, 2007. DOI: https://doi.org/10.1016/j.ijthermalsci.2006.10.003.

[7] B. B. Beya and T. Lili. Oscillatory double-diffusive mixed convection in a two-dimensional ventilated enclosure. *Int. J. Heat Mass Transf*, 50(23-24):4540–4553, 2007. DOI: https://doi.org/10.1016/j.ijheatmasstransfer.2007.03.027.

[8] M. A. Teamah and W. M. El-Maghlany. Numerical simulation of double-diffusive mixed convective flow in rectangular enclosure with insulated moving lid. *Int. J. Therm. Sci*, 49(9):1625–1638, 2010. DOI: https://doi.org/10.1016/j.ijthermalsci.2010.04.023.

[9] Y. Tizakast, M. Kaddiri, and M. Lamsaadi. Rayleigh-bénard double-diffusive mixed convection in two-dimensional rectangular cavities filled with non-newtonian fluids. *Int. J. Mech. Sci*, 227, 2022. DOI: https://doi.org/10.1016/j.ijmecsci.2022.107448.

[10] M. Gnanasekaran and A. Satheesh. Double-diffusive mixed convection with four heated square blocks for different working fluids in a square cavity, numer. *Heat Transf. B*, pages 1–25, 2023. DOI: https://doi.org/10.1080/10407790.2023.2265550.

[11] B. Sadeghi and M. Meskinfam. A direct comparison of nanosilver particles and nanosilver plates for the oxidation of ascorbic acid. *Spectrochim. Acta Part A Mol. Biomol. Spectrosc.*, 97(326-328), 2012. DOI: https://doi.org/10.1016/j.saa.2012.05.085.

[12] J. Li, X. Zhang, B. Xu, and M. Yuan. Nanofluid research and applications: A review. *Int. Commun. Heat Mass Transf*, 127:105543, 2021. DOI: https://doi.org/10.1016/j.icheatmasstransfer.2021.105543.

[13] A. Ben-Nakhi and A. J. Chamkha. Effect of length and inclination of a thin fin on natural convection in a square enclosure. *Numer. Heat Transf*, 50(4):381–399, 2006. DOI: https://doi.org/10.1080/10407780600619907.

[14] F. Talebi, A. H. Mahmoudi, and M. Shahi. Numerical study of mixed convection flows in a square lid-driven cavity utilizing nanofluid. *Int. Commun. Heat Mass Transf*, 37(1):79–90, 2010. DOI: https://doi.org/10.1016/j.icheatmasstransfer.2009.08.013.

[15] H. Nemati, M. Farhadi, K. Sedighi, E. Fattahi, and A. A. R. Darzi. Lattice boltzmann simulation of nanofluid in lid-driven cavity. *Int. Commun. Heat Mass Transf*, 37(10):1528–1534, 2010. DOI: https://doi.org/10.1016/j.icheatmasstransfer.2010.08.004.

[16] A. J. Chamkha and E. Abu-Nada. Mixed convection flow in single- and double-lid driven square cavities filled with water-al_2o_3 nanofluid: Effect of viscosity models. *Europ.J. Mech. B/Fluids*, 36: 82–96, 2012. DOI: https://doi.org/10.1016/j.euromechflu.2012.03.005.

[17] E. Abu-Nada, Z. Masoud, and H. F. Oztop. Effect of nanofluid variable properties on natural convection in enclosures. *Int. J. Thermal Sci*, 49:479–491, 2010. DOI: https://doi.org/10.1016/j.ijthermalsci.2009.09.002.

[18] T. R. R. Mahapatra, D. Pal, and S. Mondal. Influence of thermal radiation on non-darcian natural convection in a square cavity filled with fluid saturated porous medium of uniform porosity. *Nonlinear Anal-Model*, 17(2):223–237, 2012. DOI: https://doi.org/10.15388/NA.17.2.14070.

[19] T. R. Mahapatra, D. Pal, and S. Mondal. Mixed convection flow in an inclined enclosure under magnetic field with thermal radiation and heat generation. *Int. Commun. Heat Mass Transf*, 41:47–56, 2013. DOI: https://doi.org/10.1016/j.icheatmasstransfer.2012.10.028.

[20] S. Mondal and P. Sibanda. Unsteady double diffusive convection in an inclined rectangular lid-driven enclosure with different magnetic field angles and non-uniform boundary conditions. *Int. J. Heat Mass Transf*, 90:900–910, 2015. DOI: https://doi.org/10.1016/j.ijheatmasstransfer.2015.07.039.

[21] S. Mondal and P. Sibanda. Effects of buoyancy ratio on unsteady double-diffusive natural convection in a cavity filled with porous medium with non-uniform boundary conditions. *Int. J. Heat Mass Transf*, 85:401–413, 2015. DOI: https://doi.org/10.1016/j.ijheatmasstransfer.2015.01.129.

[22] S. Dinarvand, R. Hosseini, M. Abulhasansari, and I. Pop. Buongiorno's model for double-diffusive mixed convective stagnation-point flow of a nanofluid considering diffusiophoresis effect of binary base fluid. *Adv. Powder Technol*, 26(5):1423–1434, 2015. DOI: https://doi.org/10.1016/j.apt.2015.07.017.

[23] A. A. A. Arani, E. Kakoli, and N. Hajialigol. Double-diffusive natural convection of al_2o_3-water nanofluid in an enclosure with partially active side walls using variable properties. *J Mech Sci Technol*, 28:4681–4691, 2014. DOI: https://doi.org/10.1007/s12206-014-1035-0.

[24] S. M. Ahamed, S. Mondal, and P. Sibanda. Thermo-diffusion effects on unsteady mixed convection in a magneto-nanofluid flow along an inclined cylinder with a heat source, ohmic and viscous dissipation. *J. Comput. Theor. Nanosci*, 13(3):1670–1684, 2016. DOI: https://doi.org/10.1166/jctn.2016.5097.

[25] S. Hussain, H. F. Oztop, M. Jamal, and N. A. Hamdeh. Double diffusive nanofluid flow in a duct with cavity heated from below. *Int. J. Mech. Sci*, 131–132:535–545, 2017. DOI: https://doi.org/10.1016/j.ijmecsci.2017.07.057.

[26] A. I. Alsabery, M. A. Ismael, A. J. Chamkha, and I. Hashim. Mixed convection of al_2o_3-water nanofluid in a double lid-driven square cavity with a solid inner insert using buongiorno's two-phase model. *Int. J. Heat Mass Transf*, 119:939–961, 2018. DOI: https://doi.org/10.1016/j.ijheatmasstransfer.2017.11.136.

[27] R. Nath and M. Krishnan. Numerical study of double diffusive mixed convection in a backward facing step channel filled with cu-water nanofluid. *Int. J. Mech. Sci*, 153–154:48–63, 2019.
DOI: https://doi.org/10.1016/j.ijmecsci.2019.01.035.

[28] A. S. Dogonchi, A. J. Chamkha, and D. D. Ganji. A numerical investigation of magneto-hydrodynamic natural convection of cu–water nanofluid in a wavy cavity using cvfem. *J. Therm. Anal. Calorim*, 135(4):2599–2611, 2019.
DOI: https://doi.org/10.1007/s10973-018-7339-z.

[29] A. J. Chamkha and H. Al-Naser. Double-diffusive convection in an inclined porous enclosure with opposing temperature and concentration gradients. *Int. J. Therm. Sci*, 40(3):227–244, 2001.
DOI: https://doi.org/10.1016/S1290-0729(00)01213-8.

[30] M. Hashemi-Tilehnoee, A. S. Dogonchi, S. M. Seyyedi, A. J. Chamkha, and D. D. Ganji. Magnetohydrodynamic natural convection and entropy generation analyses inside a nanofluid-filled incinerator-shaped porous cavity with wavy heater block. *J. Therm. Anal. Calorim*, 141(5):2033–2045, 2020.
DOI: https://doi.org/10.1007/s10973-019-09220-6.

[31] M. A. Alomari, K. Al-Farhany, N. M. Said, and M. A. Flayyih. Numerical investigation of double-diffusive mixed convection in a split lid-driven curvilinear cavity. *Int. Commun. Heat Mass Transf*, 138:106322, 2022.
DOI: https://doi.org/10.1016/j.icheatmasstransfer.2022.106322.

[32] B. Jalili, A. Shateri, A. Akgül, A. Bariq, Z. Asadi, P. Jalili, and D. D. Ganji. An investigation into a semi-porous channel's forced convection of nano fluid in the presence of a magnetic field as a result of heat radiation. *Sci Rep*, 13:18505, 2023.
DOI: https://doi.org/10.1038/s41598-023-44275-4.

[33] R. Parveen, A. K. Hussein, T. R. Mahapatra, M. Al-Thamir, A. Abidi, M. B. B. Hamida, and R. Z. Homod F. L. andRashid. Mhd double diffusive mixed convection and heat generation/absorption in a lid-driven inclined wavy enclosure filled with a ferrofluid. *Int. J. Thermofluid*, 22:100698, 2024.
DOI: https://doi.org/10.1016/j.ijft.2024.100698.

[34] N. R. Devi, M. Gnanasekaran, A. Satheesh, P. R. Kanna, J. Taler, D. S. Kumar, D. Taler, and T. Sobota. Double-diffusive mixed convection in an inclined square cavity filled with nanofluid: A numerical study with external magnetic field and heated square blockage effects. *Case Stud. Therm. Eng*, 56:104210, 2024.
DOI: https://doi.org/10.1016/j.csite.2024.104210.

[35] C. H. Chon, K. D. Kihm, S. P. Lee, and S. U. S. Choi. Empirical correlation finding the role of temperature and particle size for nanofluid (al_2o_3) thermal conductivity enhancement. *Appl. Phys. Lett*, 87:153107, 2005.
DOI: https://doi.org/10.1063/1.2093936.

[36] C. T. Nguyen, F. Desgranges, G. Roy, N. Galanis, T. Mare, S. Boucher, and H. A. Minsta. Temperature and particle-size dependent viscosity data for water-based nanofluids-hysteresis phenomenon. *Int. J. Heat Fluid Flow*, 28:1492–1506, 2007.
DOI: https://doi.org/10.1016/j.ijheatfluidflow.2007.02.004.

[37] G. A. Sheikhzadeh, M. E. Qomi, N. Hajialigol, and A. Fattahi. Numerical study of mixed convection flows in a lid-driven enclosure filled with nanofluid using variable properties. *Results Phys*, 2:5–13, 2012.
DOI: https://doi.org/10.1016/j.rinp.2012.01.001.

[38] J. A. Esfahani and V. Bordbar. Double diffusive natural convection heat transfer enhancement in a square enclosure using nanofluids. *J. Nanotech. Eng. Med.*, 2:1–9, 2011.
DOI: https://doi.org/10.1115/1.4003794.

[39] L. C. Thomas. Heat transfer-mass transfer supplement, printice-hall. *Englewood*, 1991.